Author's Accepted Manuscript

Live imaging of collagen deposition during skin development and repair in a collagen I – GFP fusion transgenic zebrafish line

Josephine L. Morris, Stephen J. Cross, Yinhui Lu, Karl E. Kadler, Yongbo Lu, Sarah L. Dallas, Paul

Cite this article as: Josephine L. Morris, Stephen J. Cross, Yinhui Lu, Karl E. Kadler, Yongbo Lu, Sarah L. Dallas and Paul Martin, Live imaging of collagen deposition during skin development and repair in a collagen I – GFP fusion transgenic zebrafish line, *Developmental Biology,* https://doi.org/10.1016/j.ydbio.2018.06.001

This is a PDF file of an unedited manuscript that has been accepted for publication. As a service to our customers we are providing this early version of the manuscript. The manuscript will undergo copyediting, typesetting, and review of the resulting galley proof before it is published in its final citable form. Please note that during the production process errors may be discovered which could affect the content, and all legal disclaimers that apply to the journal pertain.

Live imaging of collagen deposion during skin development and repair in a collagen I – GFP fusion transgenic zebrash line

Josephine L Morris[a], Stephen J Cross[b], Yinhui Lu[c], Karl E Kadler[c], Yongbo Lu[d,e] Sarah L Dallas[d], Paul Martin[a,f,g*]

[a]School of Biochemistry, Faculty of Biomedical Sciences, University of Bristol, Bristol, UK

[b]Wolfson Bioimaging Facility, Faculty of Biomedical Sciences, University of Bristol, Bristol, UK

[c]Wellcome Trust Centre for Cell-Matrix Research, Faculty of Biology, Medicine and Health, The University of Manchester, Michael Smith Building, Oxford Road, Manchester M13 9PT, UK

[d]Department of Oral and Craniofacial Sciences, School of Dentistry, University of Missouri-Kansas City, Kansas City, Missouri, United States of America

[e]Department of Biomedical Sciences, Texas A&M University College of Dentistry, 3302 Gaston Ave., Dallas, TX 75246

[f]School of Physiology, Pharmacology and Neuroscience, Faculty of Biomedical Sciences, University of Bristol, Bristol, UK

[g]School of Medicine, Cardiff University, Cardiff CF14 4XN, UK.

* corresponding author; paul.martin@bristol.ac.uk

1

Abstract

Fibrillar collagen is a major component of many tissues but has been dificult to image *in vivo* using transgenic approaches because of problems associated with establishing cells and organisms that generate GFP-fusion collagens that can polymerise into functional ibrils. Here we have developed and characterised GFP and mCherry collagen-I fusion zebraish lines with basal epidermal-speciic expression. We use these lines to reveal the dynamic nature of collagen-I ibril deposition beneath the developing embryonic epidermis, as well as the repair of this collagen meshwork following wounding. Transmission electron microscope studies show that these transgenic lines faithfully reproduce the collagen ultrastructure present in wild type larval skin. During skin development we show that collagen I is deposited by basal epidermal cells initially in ine ilaments that are largely randomly orientated but are subsequently aligned into a cross-hatch, orthogonal sub-epithelial network by embryonic day 4. Following skin wounding, we see that sub-epidermal collagen is re-established in the denuded domain, initially as randomly orientated wisps that subsequently become bonded to the undamaged collagen and aligned in a way that recapitulates developmental deposition of sub-epidermal collagen. Crossing our GFP-collagen line against one with tdTomato marking basal epidermal cell membranes reveals how much more rapidly wound re-epithelialisation occurs compared to the re-deposition of collagen beneath the healed epidermis. By use of other tissue speciic drivers it will be possible to establish zebraish lines to enable live imaging of collagen deposition and its remodelling in various other organs in health and disease.

Keywords: collagen-I, zebraish larvae, live imaging, skin, wound healing.

2

Introducon

Collagen I is a major extracellular matrix (ECM) component within the sub-epithelial, dermal layer of the skin, where it provides structural support and acts as both a substrate for cell adhesion and migration (Van Goethem et al., 2010), and as an activator of several signalling cascades (Leitinger and Hohenester, 2007). When skin is damaged one of the key steps during repair is the deposition of ECM, in particular collagen I, to form granulation tissue which functions as a temporary replacement for the damaged dermal and sub-dermal tissues. Aberrant collagen deposition in mammalian adult skin repair leads to scarring, which can be debilitating for subsequent tissue function (Eming et al., 2014). By contrast, wounding of zebraish skin leads to deposition of a collagen "scar" which is then subsequently resolved (Richardson et al., 2013) and this may provide an ideal model to determine how collagen deposition at wound sites might be modulated to prevent ibrosis and scar formation. Here we report a zebraish line expressing luorescent collagen that can assemble into ibrils and provides opportunities to visualise the dynamics of collagen deposition *in vivo*. Previous electron microscope studies in mouse and chick have revealed some of the cellular mechanisms of collagen I deposition, and ibril alignment in developing embryonic tendons in which ibrils are all aligned in the same axis (Birk and Trelstad, 1986; Canty et al., 2004; Kalson et al., 2015) but rather little is known about collagen deposition in a more complex ECM for example, as skin is developing or when dermal tissues are rebuilt after wounding, and this is largely due to technical dificulties in live imaging these processes in model organisms. Several methodologies have been used to visualise collagen within

ixed tissues, including classic histological stains, such as Masson's Trichrome (Mori et al., 2008), or immunohistochemical staining for collagen (Richardson et al., 2013). Transmission electron microscopy offers complementary opportunities for ultrastructural analysis of collagen deposition (Starborg et al., 2013). More recently, second harmonic generation (SHG) imaging using multiphoton microscopy (Ingman et al., 2006; LaComb et al., 2008; LeBert et al., 2016; LeBert et al., 2015) and indirect visualisation of collagen through luorescently labelled collagen binding molecules (Boerboom et al., 2007; Megens et al., 2007) have begun to enable live imaging of collagen. For example,

3

collagen dynamics have been followed in live tissues *in vivo* using SHG to study cancer cell/microenvironment interactions in mouse tumours (Sahai et al., 2005); the use of collagen mimetic peptides (CMPs) (reviewed by Li and Yu, 2013) has similarly enabled detection of collagen surrounding tumours within mice (Li et al., 2012). Although these approaches have offered indirect opportunities to image collagen in tissues, greater insights are expected to come from real time visualisation of collagen deposition and ibrillogenesis in a live, *in vivo* model organism expressing luorescently tagged collagen. More recently, GFP*topaz* and mCherry-tagged collagen constructs have been generated for live imaging of collagen assembly in murine osteoblasts *in vitro*, in which the GFP-tag replaced the N-terminal propeptide of the collagen alpha2(I) chain (Lu et al., 2018). A transgenic mouse expressing GFP*topaz*-collagen under control of the 3.6kb type I collagen promoter has also been developed (Kamel-ElSayed et al., 2015). We have chosen the zebraish as a model system to probe collagen dynamics because of its genetic tractability and the optical clarity of the developing skin. By generating a transgenic zebraish line expressing collagen I fused to GFP (or mCherry) we can begin to live image deposition of collagen during skin development, and also follow collagen deposition in repairing skin; and by crossing this transgenic ish with various existing transgenic ish lines we can, for example, probe the interplay between epidermal cells and collagen I deposition at the repair site.

4

Results and Discussion

In order to live image collagen deposition in larval zebraish skin, we generated an epidermal-speciic GFP-collagen I transgenic zebraish line. It was previously presumed that due to the complex ibrillogenesis process, tagging collagens with luorescent proteins would be challenging because of the need to avoid perturbing quaternary structure and polymerisation capacity and thereby disruption of subsequent function. Basing our design on prior work of Lu and co-workers (Lu et al., 2018), we carefully considered the location for GFP insertion into the collagen molecule to ensure that the GFP label remains attached but does not signiicantly disturb collagen polymerisation and generation of functional ibrils within tissues (Kamel-ElSayed et al., 2015).

Zebraish collagen I is composed of α1a, α1b and α2 protein monomer chains, typically forming α1a(I)α1b(I)α2(I) heterotrimers (Gistelinck et al., 2016; Morvan-Dubois et al., 2003). As for mammalian collagen I, the N-propeptide of zebraish collagen a1(I) contains a von Willebrand factor type C (vWFC) like domain, whereas a2(I) lacks this domain. We did not want to perturb any

potential function that the vWFC like domain might confer so we chose the α2(I) chain for GFP labelling.

The N-terminal region of human, mouse and zebraish α2 peptide chains were aligned and compared to enable identiication of the domain boundaries (ig 1A) (Dubois et al., 2002). The 22 amino acid signal sequences of all three species demonstrated high identity (mouse and zebraish share 86%).

The N-terminal proteinase site is responsible for directing the cleavage of the pro- and telo- peptide from the major triple helical region which goes on to be utilised in trimer formation (Hojima et al., 1994). The sequence lanking the N-terminal proteinase cleavage site in all species was GNFAA|QY (with | denoting the scissile bond) (ig 1A). We removed this site by targeted mutagenesis to ensure retention of the GFP which we inserted upstream of this position.

Considering the primary structure of α2(I), we inserted GFP immediately downstream of the 22 amino acid signal sequence and upstream of the N-

5

terminal proteinase cleavage site, removing the sequence between these two positions (ig 1B). Expressing the GFP-collagen I α2 as a transgenic insertion in addition to wild type unlabelled collagen I α2 enabled production of chimeric collagen I ibrils containing both unlabelled and labelled trimers thus restricting the number of GFP molecules present on the ibril (ig 1C), and reducing potential destabilisation of ibrillar structure (Lu et al., 2018).

The GFP gene was inserted into the chosen position within zebraish *collagen I 2* cDNA, to generate *col1a2-GFP*. To enable correct folding of both collagen and GFP, a lexible glycine-serine linker was introduced at either end of the GFP. The functionality of the zebraish collagen I–GFP fusion protein was irst tested by driving expression, using a CMV promoter, within mouse ibroblasts *in vitro*. Fluorescent imaging of these cells did indeed reveal ibrillar collagen labelled with GFP (data not shown).

As described in the Methods, an expression construct was created by driving

expression of *col1a2-GFP* using the *krt1c19e* promoter (*krt19*) (Lee et al., 2014). *Krt19* drives expression in the basal epidermal cell layer which are the cells previously reported to be responsible for deposition of skin collagen I at early stages of zebrafish development (Fisher et al., 2003; Le Guellec et al., 2004; Li et al., 2011). Founder fish were generated, all of which appeared healthy and fecund, and which exhibited similar spatial expression, but variable GFP intensity between larvae. Casper zebrafish with reduced pigmentation (White et al., 2008) were used to aid in live imaging particularly since melanocytes migrate to wounds (Lévesque et al., 2013) and perturb both fluorescent and SHG imaging. Subsequent screening of F1 and F2 generation larvae for GFP expression at 4 dpf enabled selection of a transgenic fish line that demonstrated robust, bright and stable GFP-labelled collagen I fibrils within the larval skin (fig 1D). A similar cloning and selection strategy was followed to generate a complementary mCherry collagen I fish. We have previously quantified percentage of total GFP/mCherry labelling of $\alpha 2(I)$ as less than 12% in similarly generated murine cells (Lu et al., 2018); in zebrafish studies this is more difficult to directly calculate due to lack of zebrafish-specific $\alpha 2(I)$ antibodies but analysis

6

of gene expression at 5 dpf using qPCR suggests GFP labelling in our brightest fish is approximately 36% (fig S1).

Weak expression of GFP-collagen first became apparent within the skin of Tg(*krt19:col1a2-GFP*) larvae at 2 dpf and increased in intensity up to 5 dpf with particularly bright GFP expression observed first on the dorsal region of the head (fig 1D). At 2 dpf, GFP-collagen could be seen intracellularly in occasional epidermal cells and was also apparent as extracellular wispy fibrils adjacent to these cells (fig 2A). These early fibrils had no obvious orientation, just as observed by Le Guellec and co-workers when studying endogenous collagen deposition by Transmission electron microscopy (TEM) (Le Guellec et al., 2004). Previous gene expression studies indicate that endogenous *col1a2* mRNA is

expressed from the 15-somite stage (Duran et al., 2015; Gistelinck et al., 2016), with protein expression following soon after (Le Guellec et al., 2004) and so GFP-labelled collagen I, driven from the krt19 promoter at 2 dpf may be deposited where unlabelled wild type ibrils have already been laid down.

At 3 dpf we see GFP-collagen I ibrils beneath the lank epidermis beginning to remodel into a cross-hatched pattern with ibrils arranged perpendicular to each other and by 4 dpf the ibril orthogonality was fully evident (ig 2B). Similarly, for mCherry-collagen I transgenic ish, a regular orthogonal pattern developed (fig S3B). Orthogonal GFP-collagen I labelling persists in the juvenile and adult zebraish (ig S2); however, at these later stages labelling was restricted to the scale-layer. As expected, since the *krtt1c19e* promoter does not drive expression in the larval in fold epithelium during zebraish development (Lee et al., 2014), GFP labelling did not extend into the ins within larval transgenic ish. We believe that the GFP luorescence relects location of basal epidermal-derived collagen,; however, some of the labelling within the Tg(*krt19:col1a2-GFP*) ish might be ectopic due to the use of the strong non-collagen I, keratin promoter.

Utilising a modiied version of the Fiji 'Directionality' plugin (Tinevez, 2010), a Fourier transform-based method, enabled analysis of the alignment of the ine collagen I-containing ibrils. Using the output from this plugin, further analyses

7

(Sun et al., 2015) were performed which allowed us to compare alignment index (AI) between maximum projected images generated by confocal microscopy over a range of time points. This analysis demonstrated that AI increased from 2 dpf (0.21 ± 0.08) to 3 dpf (0.58 ± 0.08) relecting increasing levels of collagen I orthogonality (ig 2C), which was then maintained from 4 dpf onwards.

TEM studies of our Tg(*krt19:col1a2-GFP*) ish conirmed that the orthogonal ibrils within 5 dpf larval ish skin were orientated in plywood-like layers as previously demonstrated for wild type ish (Le Guellec et al., 2004) (ig 2D, E) suggesting that the GFP tag (or removal of N-terminal pro- and telo-peptide) does not signiicantly alter ibril patterning.

As well as the orthogonal sub-epidermal collagen network, we also observed protrusions of collagen I extending from this meshwork deep into tendinous myosepta, separating the muscle blocks (ig 2F, S3A), as previously described in EM studies (Charvet et al., 2011). These data strongly indicate that the myosepta receive at least some contribution from epithelial cells although what proportion of the collagen in this structure might also be derived from ibroblasts (Bader et al., 2009; Kudo et al., 2004) cannot be determined from our studies.

In the tail of our transgenic ish we observe lateral tethers and bilateral, rod-shaped structures (ig 2H; also seen by second harmonic generation (SHG) imaging, ig S4) which we presume are developing tail tendons as previously reported in tuna ish (Shadwick et al., 2002). In addition, in the head there are numerous deep protrusions tethering the skin to underlying structures of the developing craniofacial skeleton (ig 2G) (Chen and Galloway, 2014).

We directly compared confocal images of the GFP-collagen I transgenic ish with images acquired from the same larvae by SHG (ig S5) and while both reveal some details of the orthogonal collagen structure, SHG imaging led to considerable interference from the deeper muscle tissue while GFP-collagen I

8

labelling allowed creation of maximum projection images enabling us to observe the ibril structure at high resolution throughout the curved zebraish skin.

We were concerned that addition of GFP at the N-terminal might subtly alter ibrillar structure, similar to that seen in Ehlers Danlos Syndrome Type VIIB (EDS VIIB), where the N-proteinase cleavage site is not present on collagen I α2 chains causing the retention of the N-terminal propepetide (Eyre et al., 1985; Holmes et al., 1993; Watson et al., 1992). However, our transgenic ish line does not appear to exhibit any obvious skin symptoms of EDS VIIB, such as skin laxity.

That said, whilst the GFP-tagged collagen construct leads to appropriate in vivo localisation of the GFP-collagen fusion protein, and ibrils appear normal by TEM and SHG imaging approaches, we cannot exclude more subtle differences in traficking, processing, secretion or crosslinking due to the GFP tag. However, even with these potential limitations, the construct clearly provides a powerful and useful tool for *in vivo* collagen imaging.

To examine the dynamics of collagen deposition in a repairing skin wound we made stab wounds, with a hypodermic needle, to 4 dpf GFP-collagen larval ish (fig 3A) and observed GFP-collagen at various time points post-wounding. Immediately post-wounding confocal microscopy conirmed that sub-epidermal collagen I at the wound site was now completely absent (ig 3B, C inset). Its margins at the wound edge were raised and wrinkled as if released from tension at the time of wounding (ig 3C inset). Indeed, previous TEM studies of mouse embryo wound healing reveal a similar "elastic" retraction of the ECM following wounding (McCluskey et al., 1993). Crossing the GFP-collagen I ish against a line expressing membrane tethered tdTomato in the basal epidermal cells allows us to compare repair of the epidermis versus the epidermal-derived collagen at the wound site. The epidermal wound seals very rapidly, generally in less than an hour (ig 3B, S6, Movie 1), whereas the "defect" in the collagen I layer remained absent of collagen for up to 3 days post injury (dpi; ig 3D), with a clear edge delineating where the wound had been. Movies of several hours duration (Movie

9

1) can be made to capture collagen dynamics, without signiicant bleaching or ill health of the larva, but since collagen remodelling in the wound takes several days, the images we show are taken from several individual ish.

We observed new GFP-collagen I irst being deposited in the wound gap from 4 dpi (ig 3D), after rapid closure of the epidermal wound (ig 3B, Movie 1). This

new collagen was wispy and more randomly aligned than the orthogonal structure of adjacent unwounded skin collagen. Using the Fourier based methods described above, we quantiied collagen orientation and showed that the AI (collagen alignment index) at 5 dpi was 0.34 ± 0.15 (compared to 0.60 ± 0.11 unwounded; ig 3J). Between 4 and 7 dpi, the quantity of irregular collagen in the wound domain increased, although, there remained a clear interface between this recently deposited wound collagen and the remaining collagen plywood structure surrounding the wound. At this interface we see wispy linkers, suggesting that new collagen may be deposited/fused onto the existing ibrils to extend the repairing matrix out into the wound domain (ig 3E).

By 9 to 11 dpi, the sub-epidermal collagen I within the wound site appeared to become more intimately bonded to the neighbouring unwounded matrix with some regions evolving towards a pre-wound orthogonal pattern (ig 3G,H), which was relected in a gradual increase in AI throughout the timeframe of wound healing (ig 3J). By 16 dpi the wound site was increasingly dificult to locate because for many ish the collagen at the wound site had fully resolved back to near perfect pre-wound orthogonal pattern leaving no trace of a defect in the sub-epidermal meshwork, which was conirmed by comparable alignment indices (0.50 ± 0.13 injured, 0.54 ± 0.10 uninjured for 16 dpi) (ig 3I,J).

At sites where the myoseptum had been damaged, the "repair" collagen is not always perfectly regenerated in the typical chevron pattern as initially laid down during development, and these defects often remain beneath the healed skin. Separate from the myoseptum we also observe GFP-collagen deposits that lie horizontally just beneath the epidermis and appear to bind the adjacent undamaged myosepta together, and also deeper deposits within the muscle layer, suggesting that these might function as "adhesions" for the repairing epidermis at the wound site (ig 3K,L).

10

In mammalian skin repair, after wound-re-epithelialisation, the deeper dermal collagen that eventually forms a wound scar is formed of tight aligned bundles,

rather than the more random, "basket-weave" fibrils of unwounded dermis, and this scar collagen is not subsequently remodelled to the original "unwounded" pattern (Cash et al., 2014; Eming et al., 2014). In adult zebraish skin and heart, scar collagen is also deposited after damage, but is subsequently remodelled to leave behind a perfectly regenerated tissue without scar (Chablais et al., 2011; González-Rosa et al., 2011; Richardson et al., 2013). Further study of this regenerative healing of zebraish tissues and a better understanding of how non-scar collagen is deposited beneath the epidermis may provide insights into how to modulate the mammalian repair process to reduce scarring.

We have demonstrated that by combining our GFP-collagen and mCherry-collagen ish with other established reporter ish we can exploit the unique live imaging opportunities available in larval ish to probe the processes involved in collagen deposition and remodelling. By crossing our GFP-collagen ish with one labelling basal epidermal cell membranes, we have been able to compare the healing of epidermis versus the re-establishment of collagen beneath the epidermis and reveal the dramatically different timecourse of healing for these two layers. Similarly, we have crossed the mCherry-collagen I ish against the ET37 (Parinov et al., 2004) enhancer trap line, labelling ibroblast-like cells (Lee et al., 2013) with eGFP, in order to observe the relationship between inlux of these cells and epidermal collagen I deposition (ig S3C); as for re-epithelialisation, ibroblast-like cell inlux occurs rapidly compared to matrix deposition. In the future, by crossing the GFP (or mCherry)-collagen-I lines against other ish lines, it will be possible to analyse the relationship between sub-epidermal collagen deposition and the wound inlammatory response (see Movie 2), or to compare the timecourse of deposition of the various matrix components of the basement membrane. Additionally, it would also be possible to study collagen dynamics within other tissues, by driving the expression of this GFP-collagen construct using other tissue-speciic promoters.

11

Materials and Methods

Adult zebraish (*Danio rerio*) were maintained and crossed as previously described (Westerield, 2007). All experiments were conducted with local ethical approval from the University of Bristol and in accordance with UK Home Ofice regulations. Zebraish lines utilised were, Tg(*krt19:TdTomatoCAAX*) (epidermis and collagen I) and Tg(*mpeg1.1:mcherry)* (Ellett et al., 2011) (macrophages and collagen I) which were out-crossed to Tg*(krt19:col1a2-GFP)* for dual-labelling experiments and ET37 (Parinov et al., 2004) which was out-crossed to Tg*(krt19:col1a2-mCherry)* to enable imaging of epidermal-derived collagen I alongside ibroblasts-like cells. All experiments were performed on Tg*(krt19:col1a2-GFP/mCherry)* homozygous ish and all ish were on a Casper background (White et al., 2008).

The sequences of zebraish collagen I   chains were compared to those of mouse and human using Clustalo alignments and literature searches (Dubois et al., 2002; Le Guellec et al., 2004) in order to establish conserved sequences and domain boundaries. Accession numbers for sequence comparison were BC071278.1, J03464 and X58251.1, for zebraish, human and mouse respectively.

For generation of the GFP-collagen fusion protein, we followed the approach of Lu and co-workers in which the GFP tag replaced the N-terminal propeptide and telopeptide of murine alpha2(I) procollagen (Lu et al., 2018). Our strategy was to express the zebraish GFP-collagen I α2 under control of a keratin promoter (Krtt1c19e (Lee et al., 2014)) to drive expression in basal epidermal cells. Plasmid containing zebraish *collagen type I alpha 2* chain (*col1a2*) cDNA, pCMVSport6.1-*Zcol1a2*, was obtained from Source Bioscience. Mutagenic PCR, using primers Zcol1a007 (GGATCCacatgatgctaggtacgaagtcactg, BamHI in capitals) and Zcol1a029 (cagtatgatggcgctaaaggacct), was used to remove the pro-

12

and telo- peptide from the N-terminal of the *col1a2* gene and to insert a BamHI restriction site at site of GFP insertion.

DNA ampliied by PCR, using primers eGFP001 and eGFP003 (cgtgcgGGATCCatggtgagcaagggcgagg, actcgaGGATCCcttgtacagctcgtccatgcc, respectively, BamHI in capitals) and template pME-GFP (Kwan et al., 2007), was puriied by gel extraction from an agarose gel, digested and ligated into similarly BamHI digested *col1a2*. Colony PCR was utilised to screen colonies for insertion of GFP in the correct orientation, generating plasmid pCMVSport6.1-*Zcol1a2-GFP*. Plasmid pME-*Zcol1a2GFP* was generated utilising a Gateway BP (Invitrogen) reaction along with pDONR221 and pCMVSport6.1-*Zcol1a2-GFP*.

A destination vector, pDEST-*krt19:col1a2-GFP*, was generated utilising pME-*Zcol1a2GFP,* p5E-*krtt1c19e*; (Lee et al., 2014), p3E-pA, pDESTTol2pA2 from the Tol2kit (Kwan et al., 2007), in a LR Clonase II Plus enzyme mediated LR Gateway recombination reaction (Invitrogen). Sequencing conirmed generation of all plasmids.

A 1 nl volume of expression vector pDEST-*krt19:col1a2GFP* construct at 62.5 ng µl^{-1}, together with 50 ng µl^{-1} puriied Tol2 mRNA was microinjected into Casper zebraish one cell stage embryos, as previously described (Hall et al., 2007). Injected larvae were screened for GFP expression at 3-7 days post injection by luorescent microscopy and GFP positive larvae were grown to sexual maturity and screened for germline transmission. By screening successive generations a transgenic line was established which stably expressed bright GFP labelled collagen I within the skin (ig 1D). An identical process was adopted for generation of a collagen I 2 - mCherry expressing line utilising a pDEST-*krt19:col1a2mCherry* construct as outlined in Supplementary Methods.

Four days post fertilisation larvae were wounded with a 30G hypodermic needle on their lank directly above the cloaca. For imaging, ish were mounted on their sides in 1% low gelling temperature agarose (Sigma), in a glass bottomed dish, illed with Danieau's solution with 0.1 mg ml $^{-1}$ tricaine anaesthetic. Leica TCS SP8

Live imaging of collagen deposition during skin development and repair in a collagen I – GFP fusion transgenic zebrafish line   19/06/2018, 11:34

13

AOBS confocal laser scanning microscope attached to a Leica DMi8 inverted epiluorescence microscope equipped with a 65 mW Ar laser along with 'hybrid' GaAsP detectors was utilised to image larval ish. Fish were imaged using a 63x 1.3 NA glycerol objective.

Second harmonic generation (SHG) microscopy was performed using a Leica SP8 AOBS confocal laser tandem scanning microscope attached to a Leica DM6000 upright epiluorescence microscope with tuneable Spectra Physics DeepSee dual beam pre-chirped 680-1300 nm multiphoton laser, set to 880 nm for SHG. A 25x HC Fluotar 0.95 NA water-dipping objective was used.

Imaging of wounded juvenile ish was performed on the same Leica SP8 AOBS confocal microscope but using lasers for single photon excitation (Argon and 561 nm) along with the internal 'hybrid' GaAsP detectors and transmitted light detector. A 25x HC Fluotar 0.95 NA water-dipping objective was used. Leica microscopes were interfaced with the LAS-AF software (Leica Microsystems, Wetzlar, Germany). Timelapse microscopy to generate movies of wound closure commenced 30 minutes or 3 days post injury with images taken every 10-30 minutes for 15-17.5 hours. Images were processed using Fiji using maximum projection, 3D viewer for 3D reconstructions (Schmid et al., 2010) and bleach correction plugins (Miura et al., 2014).

Maximum intensity and 3D projections were performed using Fiji (Schindelin et al., 2012) or Volocity (PerkinElmer). Analysis of collagen ibril orientation was performed using the 'Directionality' plugin (Tinevez, 2010) for ImageJ (Schneider et al., 2012) with amendments to split the results into angle ranges of 0-90 and 90-180 degrees. Also added to the plugin was an algorithm to report Alignment Index (AI) (Sun et al., 2015) for each of the angle ranges calculated using the following equation,

$$\overline{N}$$

is the mean orientation angle and N is

Where is number of angular measurements. An AI=1 would relect no angular dispersion and thus full ibril alignment whereas AI=0 would indicate an entirely

14

randomly alignment of ibrils. Prior to calculation of AI, background was subtracted from the angular histogram to improve signal to noise. The plugin and source code are available within supplementary information.

Output from this plugin was further analysed using one-way ANOVA with Tukey's multiple comparisons test for developmental measurements and t tests for wounded versus unwounded timecourse (Graphpad Prism 7.0).

Culled larval zebraish were ixed in 0.05 M sodium cacodylate buffer (pH 7.2) containing 4% (v/v) glutaraldehyde, 1% (v/v) paraformaldehyde, 1 mM magnesium sulphate and1% sucrose overnight at 4°C. Ultrathin sections (70 nm thick) were prepared for electron microscopy as described previously (Canty et al., 2004).

15

Acknowledgements

Supplementary Informaon

DNA ampliied by PCR, using primers Zcol1a051 (cgtgcgACCGGTctggacacgcagtcaagggaacct, AgeI in capitals) and Zcol1a052 (actcgATCGATcggaacaatggacatgctttt, ClaI in capitals) and template pME-Zcol1a2-

mCherry (generated as for pME-*zcol1a2GFP*), was puriied by gel extraction from an agarose gel, digested with AgeI-HF/ClaI/DpnI and ligated into similarly AgeI-HF/ClaI/AnP digested and gel-puriied pDEST-*krt19:col1a2-GFP*. Colony PCR was utilised to screen colonies for insertion of mCherry and production of pDEST-*krt19:col1a2-mCherry* was conirmed by DNA sequencing.

16

A stable Tg(*krt19:tdTomatoCAAX*) transgenic zebraish line was produced using constructs generated using the Tol2 kit (Kwan et al., 2007), with the described *krttc19e* promoter fragment (Lee et al., 2014), along with pME-*tdTomatoCAAX* (a gift from Dr. Thomas Ramezani), followed by standard injection and screening procedures.

Fish were anaesthetised with 0.1 mg ml^{-1} tricaine in Danieau's solution, most of the liquid was removed and ish were laid out on a 10 cm dish. A MZ10F Leica wideield microscope equipped with a Leica DFC7000T camera and Leica LAS software was used to capture both brightield and GFP luorescent images. These images were overlaid using Fiji. Confocal imaging was performed as for larval zebraish.

RNA was extracted from twenty 5 dpf zebraish using TRIzol and isopropanol precipitation. DNase treatment and cDNA irst strand synthesis was performed using Maxima First Strand cDNA Synthesis Kit (ThermoFisher), using 0.4 μg RNA following the manufacturers protocol. Quantitative PCR was performed on cDNA using a SYBR Green PCR kit (Qiagen) in an Agilent MX3005P QPCR cycler using primer pairs zcol1a057/058 (AGGGACCAAAAGGACCCAGA and CAGCGAAGTTTCCACCAAGAC respectively) to amplify endogenous *col1a2* only and eGFP010/012 (CTCGTGACCACCCTGACCTA and GGCGGACTTGAAGAAGTCGT

respectively) to amplify *eGFP* within *col1a2GFP* only. Ampliication of *EF1a* (primers CTGGTTCAAGGGATGGAAGA and GAGACTCGTGGTGCATCTCA) was used as reference.

17

Graph showing qPCR data indicating expression of *col1a2-GFP* is approximately 36% compared to *col1a2* in zebraish larvae at 5 dpf.

(A) Wideield bright ield and luorescent images of 28 dpf and (C) 6 month pf (mopf) GFP-collagen I ish showing they remain GFP positive, whereas only the gut is autoluorescent in non-transgenic ish. Region imaged by confocal indicated by white box. (B, D) Maximum projection confocal images demonstrate the GFP-collagen I is still orthogonal in nature, but it is located in the scale-layer. Scale bars: A = 1mm; B,D = 25 μm.

(A) Equivalent single z-plane confocal and SHG (A') image of a 10 dpf Tg(*krt19:col1a2-GFP*) zebraish, indicating myoseptal labelling (arrowhead in A'). (B,C) A maximum projection confocal images of

Tg(*krt19:col1a2-mcherry*), ET37 double transgenic zebraish to show relationship of epidermal-derived collagen I (red), with inlux of ibroblasts-like cells (green) to wound, just prior to (B) and 2 dpi (C). Scale bars = 25 μm.

. (A) Maximum projection confocal image of GFP-collagen I transgenic zebraish. (B) Maximum projection of forward second harmonic generation (SHG) microscopy image. Tail tendon indicated by arrowhead. (C) Maximum projection of backward SHG microscopy image. Developing actinotrichia in the tail in are also labelled in B and C (but not A). (D) Overlay of GFP, forward and backward SHG.

18

(A) A maximum projection confocal image and (B) single z-plane image of a 10 dpf GFP-collagen I transgenic ish directly compared to a single z-plane signal from a second harmonic generation (SHG) microscopy image of the same ish (C). (D) A single z-plane SHG microscopy image of a non-transgenic zebraish. M, muscle ibres; O, orthogonal collagen fibrils. Scale bar = 15 μm.

Still images from repairing wounds to the lanks of 4 dpf Tg*(krt19:col1a2-GFP),* Tg*(krt19:tdTomatoCAAX)* double transgenic ish to reveal relative time course of repair of the cellular versus matrix layers. Scale bar = 25 μm.

Stab wounds were made to the lanks of 4 dpf Tg*(krt19:col1a2-GFP),* Tg*(krt19:tdTomatoCAAX)* double transgenic ish. Max projection confocal

timelapse microscopy from approximately 0.5 to 17.5 hours post injury indicates how wound re-epithelialisation is complete long before collagen matrix is repaired. Scale bar = 25 μm.

3D reconstruction of confocal timelapse imaging reveals macrophages migrating within the newly deposited epidermal-derived collagen I matrix in a Tg(*krt19:col1a2-GFP*), Tg(*mpeg1.1:mcherry*) double transgenic ish at 3 dpi. Even over a 15 hr period very little new collagen is deposited indicating the slow timecourse of this process. Scale bar = 25 μm.

19

References

Bader, H.L., Keene, D.R., Charvet, B., Veit, G., Driever, W., Koch, M., Ruggiero, F., 2009. Zebraish collagen XII is present in embryonic connective tissue sheaths (fascia) and basement membranes. Matrix Biology 28, 32-43.
Birk, D.E., Trelstad, R.L., 1986. Extracellular compartments in tendon morphogenesis: collagen ibril, bundle, and macroaggregate formation. The Journal of cell biology 103, 231-240.
Boerboom, R.A., Krahn, K.N., Megens, R.T., van Zandvoort, M.A., Merkx, M., Bouten, C.V., 2007. High resolution imaging of collagen organisation and synthesis using a versatile collagen speciic probe. Journal of structural biology 159, 392-399.
Canty, E.G., Lu, Y., Meadows, R.S., Shaw, M.K., Holmes, D.F., Kadler, K.E., 2004. Coalignment of plasma membrane channels and protrusions (ibripositors) speciies the parallelism of tendon. The Journal of cell biology 165, 553-563.
Cash, J.L., Bass, M.D., Campbell, J., Barnes, M., Kubes, P., Martin, P., 2014.

Resolution mediator chemerin15 reprograms the wound microenvironment to promote repair and reduce scarring. Current Biology 24, 1406-1414.

Chablais, F., Veit, J., Rainer, G., Jaźwińska, A., 2011. The zebrafish heart regenerates after cryoinjury-induced myocardial infarction. BMC developmental biology 11, 21.

Charvet, B., Malbouyres, M., Pagnon-Minot, A., Ruggiero, F., Le Guellec, D., 2011. Development of the zebraish myoseptum with emphasis on the myotendinous junction. Cell and tissue research 346, 439-449.

Chen, J.W., Galloway, J.L., 2014. The development of zebraish tendon and ligament progenitors. Development 141, 2035-2045.

Dubois, G.M., Haftek, Z., Crozet, C., Garrone, R., Le Guellec, D., 2002. Structure and spatio temporal expression of the full length DNA complementary to RNA coding for α2 type I collagen of zebrafish. Gene 294, 55-65.

Duran, I., Csukasi, F., Taylor, S., Krakow, D., Becerra, J., Bombarely, A., Mari-Beffa, M., 2015. Collagen duplicate genes of bone and cartilage participate during regeneration of zebraish in skeleton. Gene Expression Patterns 19, 60-69.

Ellett, F., Pase, L., Hayman, J.W., Andrianopoulos, A., Lieschke, G.J., 2011. mpeg1 promoter transgenes direct macrophage-lineage expression in zebraish. Blood 117, e49-e56.

Eming, S.A., Martin, P., Tomic-Canic, M., 2014. Wound repair and regeneration: mechanisms, signaling, and translation. Science translational medicine 6, 265sr266-265sr266.

Eyre, D., Shapiro, F., Aldridge, J., 1985. A heterozygous collagen defect in a variant of the Ehlers-Danlos syndrome type VII. Evidence for a deleted amino-telopeptide domain in the pro-alpha 2 (I) chain. Journal of Biological Chemistry 260, 11322-11329.

Fisher, S., Jagadeeswaran, P., Halpern, M.E., 2003. Radiographic analysis of zebraish skeletal defects. Developmental biology 264, 64-76.

20

Gistelinck, C., Gioia, R., Gagliardi, A., Tonelli, F., Marchese, L., Bianchi, L., Landi, C., Bini, L., Huysseune, A., Witten, P., 2016. Zebraish Collagen Type I: Molecular and Biochemical Characterization of the Major Structural Protein in Bone and Skin. Scientiic reports 6.

González-Rosa, J.M., Martín, V., Peralta, M., Torres, M., Mercader, N., 2011. Extensive scar formation and regression during heart regeneration after cryoinjury in zebraish. Development 138, 1663-1674.

Hall, C., Flores, M.V., Storm, T., Crosier, K., Crosier, P., 2007. The zebraish lysozyme C promoter drives myeloid-speciic expression in transgenic ish. BMC developmental biology 7, 42.

Hojima, Y., Mörgelin, M., Engel, J., Boutillon, M.-M., van der Rest, M., McKenzie, J., Chen, G.-C., Rai, N., Romanic, A.M., Prockop, D.J., 1994. Characterization of type I procollagen N-proteinase from fetal bovine tendon and skin. Puriication of the 500-kilodalton form of the enzyme from bovine tendon. Journal of Biological Chemistry 269, 11381-11390.

Holmes, D., Watson, R., Steinmann, B., Kadler, K., 1993. Ehlers-Danlos syndrome

type VIIB. Morphology of type I collagen fibrils formed in vivo and in vitro is determined by the conformation of the retained N-propeptide. Journal of Biological Chemistry 268, 15758-15765.

Ingman, W.V., Wyckoff, J., Gouon-Evans, V., Condeelis, J., Pollard, J.W., 2006. Macrophages promote collagen fibrillogenesis around terminal end buds of the developing mammary gland. Developmental Dynamics 235, 3222-3229.

Kalson, N.S., Lu, Y., Taylor, S.H., Starborg, T., Holmes, D.F., Kadler, K.E., 2015. A structure-based extracellular matrix expansion mechanism of fibrous tissue growth. Elife 4, e05958.

Kamel-ElSayed, S.A., Tiede-Lewis, L.M., Lu, Y., Veno, P.A., Dallas, S.L., 2015. Novel approaches for two and three dimensional multiplexed imaging of osteocytes. Bone 76, 129-140.

Kudo, H., Amizuka, N., Araki, K., Inohaya, K., Kudo, A., 2004. Zebrafish periostin is required for the adhesion of muscle fiber bundles to the myoseptum and for the differentiation of muscle fibers. Developmental biology 267, 473-487.

Kwan, K.M., Fujimoto, E., Grabher, C., Mangum, B.D., Hardy, M.E., Campbell, D.S., Parant, J.M., Yost, H.J., Kanki, J.P., Chien, C.B., 2007. The Tol2kit: a multisite gateway based construction kit for Tol2 transposon transgenesis constructs. Developmental Dynamics 236, 3088-3099.

LaComb, R., Nadiarnykh, O., Campagnola, P.J., 2008. Quantitative Second Harmonic Generation Imaging of the Diseased State Osteogenesis Imperfecta: Experiment and Simulation. Biophysical Journal 94, 4504-4514.

Le Guellec, D., Morvan-Dubois, G., Sire, J.-Y., 2004. Skin development in bony fish with particular emphasis on collagen deposition in the dermis of the zebrafish (Danio rerio). International Journal of Developmental Biology 48, 217-232.

LeBert, D., Squirrell, J., Huttenlocher, A., Eliceiri, K., 2016. Second harmonic generation microscopy in zebrafish. Methods in cell biology 133, 55-68.

LeBert, D.C., Squirrell, J.M., Rindy, J., Broadbridge, E., Lui, Y., Zakrzewska, A., Eliceiri, K.W., Meijer, A.H., Huttenlocher, A., 2015. Matrix metalloproteinase 9 modulates collagen matrices and wound repair. Development 142, 2136-2146.

Lee, R.T., Asharani, P., Carney, T.J., 2014. Basal keratinocytes contribute to all strata of the adult zebrafish epidermis. PloS one 9, e84858.

21

Lee, R.T.H., Knapik, E.W., Thiery, J.P., Carney, T.J., 2013. An exclusively mesodermal origin of fin mesenchyme demonstrates that zebrafish trunk neural crest does not generate ectomesenchyme. Development 140, 2923-2932.

Leitinger, B., Hohenester, E., 2007. Mammalian collagen receptors. Matrix Biology 26, 146-155.

Lévesque, M., Feng, Y., Jones, R.A., Martin, P., 2013. Inflammation drives wound hyperpigmentation in zebrafish by recruiting pigment cells to sites of tissue damage. Disease models & mechanisms 6, 508-515.

Li, Q., Frank, M., Thisse, C.I., Thisse, B.V., Uitto, J., 2011. Zebrafish: a model system to study heritable skin diseases. Journal of Investigative Dermatology 131, 565-571.

Li, Y., Foss, C.A., Summerfield, D.D., Doyle, J.J., Torok, C.M., Dietz, H.C., Pomper,

M.G., Yu, S.M., 2012. Targeting collagen strands by photo-triggered triple-helix hybridization. Proceedings of the National Academy of Sciences 109, 14767-14772.

Li, Y., Yu, S.M., 2013. Targeting and mimicking collagens via triple helical peptide assembly. Current opinion in chemical biology 17, 968-975.

Lu, Y., Kamel El Sayed, S.A., Wang, K., Tiede Lewis, L.M., Grillo, M.A., Veno, P.A., Dusevich, V., Phillips, C.L., Bonewald, L.F., Dallas, S.L., 2018. Live Imaging of Type I Collagen Assembly Dynamics in Osteoblasts Stably Expressing GFP and mCherry Tagged Collagen Constructs. Journal of Bone and Mineral Research.

McCluskey, J., Hopkinson-Woolley, J., Luke, B., Martin, P., 1993. A study of wound healing in the E11. 5 mouse embryo by light and electron microscopy. Tissue and Cell 25, 173-181.

Megens, R.T., oude Egbrink, M.G., Cleutjens, J.P., Kuijpers, M.J., Schiffers, P.H., Merkx, M., Slaaf, D.W., Van Zandvoort, M.A., 2007. Imaging collagen in intact viable healthy and atherosclerotic arteries using luorescently labeled CNA35 and two-photon laser scanning microscopy. Molecular imaging 6, 247-260.

Miura, K., Rueden, C., Hiner, M., Schindelin, J., Rietdorf, J., 2014. ImageJ Plugin CorrectBleach V2.0.2, V2.0.2 ed.

Mori, R., Shaw, T.J., Martin, P., 2008. Molecular mechanisms linking wound inlammation and ibrosis: knockdown of osteopontin leads to rapid repair and reduced scarring. Journal of Experimental Medicine 205, 43-51.

Morvan-Dubois, G., Le Guellec, D., Garrone, R., Zylberberg, L., Bonnaud, L., 2003. Phylogenetic Analysis of Vertebrate Fibrillar Collagen Locates the Position of Zebrafish α3(I) and Suggests an Evolutionary Link Between Collagen α Chains and Hox Clusters. J Mol Evol 57, 501-514.

Parinov, S., Kondrichin, I., Korzh, V., Emelyanov, A., 2004. Tol2 transposon-mediated enhancer trap to identify developmentally regulated zebraish genes in vivo. Developmental Dynamics 231, 449-459.

Richardson, R., Slanchev, K., Kraus, C., Knyphausen, P., Eming, S., Hammerschmidt, M., 2013. Adult zebraish as a model system for cutaneous wound-healing research. Journal of Investigative Dermatology 133, 1655-1665.

Sahai, E., Wyckoff, J., Philippar, U., Segall, J.E., Gertler, F., Condeelis, J., 2005. Simultaneous imaging of GFP, CFP and collagen in tumors in vivousing multiphoton microscopy. BMC Biotechnology 5, 1-9.

Schindelin, J., Arganda-Carreras, I., Frise, E., Kaynig, V., Longair, M., Pietzsch, T., Preibisch, S., Rueden, C., Saalfeld, S., Schmid, B., Tinevez, J.-Y., White, D.J.,

22

Hartenstein, V., Eliceiri, K., Tomancak, P., Cardona, A., 2012. Fiji: an open-source platform for biological-image analysis. Nat Meth 9, 676-682.

Schmid, B., Schindelin, J., Cardona, A., Longair, M., Heisenberg, M., 2010. A high-level 3D visualization API for Java and ImageJ. BMC Bioinformatics 11, 274.

Schneider, C.A., Rasband, W.S., Eliceiri, K.W., 2012. NIH Image to ImageJ: 25 years of image analysis. Nature Methods 9, 671.

Shadwick, R.E., Rapoport, H.S., Fenger, J.M., 2002. Structure and function of tuna tail tendons. Comparative Biochemistry and Physiology Part A: Molecular &

Integrative Physiology 133, 1109-1125.

Starborg, T., Kalson, N.S., Lu, Y., Mironov, A., Cootes, T.F., Holmes, D.F., Kadler, K.E., 2013. Using transmission electron microscopy and 3View to determine collagen ibril size and three-dimensional organization. Nature protocols 8, 1433-1448.

Sun, M., Bloom, A.B., Zaman, M.H., 2015. Rapid quantiication of 3D collagen iber alignment and iber intersection correlations with high sensitivity. PloS one 10, e0131814.

Tinevez, J.-Y., 2010. Directionality (Fiji), v2.0 ed. ImageJ, http://imagej.net/Directionality, p. ImageJ plugin to infer the preferred orientation of structures present in the input image.

Van Goethem, E., Poincloux, R., Gauffre, F., Maridonneau-Parini, I., Le Cabec, V., 2010. Matrix architecture dictates three-dimensional migration modes of human macrophages: differential involvement of proteases and podosome-like structures. The journal of immunology 184, 1049-1061.

Watson, R.B., Wallis, G.A., Holmes, D.F., Viljoen, D., Byers, P.H., Kadler, K.E., 1992. Ehlers Danlos syndrome type VIIB. Incomplete cleavage of abnormal type I procollagen by N-proteinase in vitro results in the formation of copolymers of collagen and partially cleaved pNcollagen that are near circular in cross-section. Journal of Biological Chemistry 267, 9093-9100.

Westerield, M., 2007. The Zebraish Book. A Guide for the Laboratory Use of Zebraish (Danio rerio), 5th Edition ed. University of Oregon Press, Eugene.

White, R.M., Sessa, A., Burke, C., Bowman, T., LeBlanc, J., Ceol, C., Bourque, C., Dovey, M., Goessling, W., Burns, C.E., 2008. Transparent adult zebraish as a tool for in vivo transplantation analysis. Cell stem cell 2, 183-189.

23

(A) The N-

terminal regions of zebrafish, mouse and human collagen I α2 chains were aligned to determine the N-terminal proteinase cleavage site (red line) and identify the optimal GFP insertion site. (B) By inserting GFP in place of the N-terminal pro- and telo- peptide and removing the N-terminal proteinase site, GFP was retained on the α2 monomer. (C) GFP-tagged α2 trimerises with unlabelled α1a and α1b monomers and fibrillogenesis occurs with labelled and unlabelled trimers. (D) Tg*(krt19:col1a2-GFP)* transgenic ish exhibit GFP labelling within lank skin when compared to control, non-transgenic zebraish where only the gut shows faint autoluorescence. D is composed of a 4-image tilescan confocal image of a 4 dpf zebraish. Scale bar = 0.5mm.

(A) In the region of lank indicated by the box in larval schematic, the earliest GFP-collagen I is seen at 2 dpf in maximum projection confocal images of Tg*(krt19:col1a2-GFP)* transgenic zebraish; GFP-collagen is seen within sporadic cells (arrowhead), and in some adjacent patches exhibiting the beginning of orthogonal patterning (arrow), as well as within myosepta (open arrowhead). (B) At 4 dpf orthogonal structure is fully evident. (C) Quantiication of collagen alignment index (AI) over developmental time. Plotted as mean ± SD and analysed using a one-way ANOVA, ****$p<0.0001$, n=10-16 ish. (D, E) Transmission electron microscopy (TEM) of lank skin of 5 dpf Tg*(krt19:col1a2-GFP)* transgenic (D) and non-transgenic (E) larvae (with high magniication inset, D', E') reveals the orthogonal layering of collagen I; arrows indicate collagen ibril; arrowhead indicates adjacent orthogonal layer of collagen ibrils; n, nucleus; bc, basal cell cytoplasm; asterisk, basement membrane; line denotes collagen I layer. (F) GFP-collagen I tethers extend deep into the tissue of the 3 dpf ish as anchors to the underlying tissue within the myoseptum (asterisks); (G) Similarly, collagenous tethers link the epidermis to deep structures in the head, as for example around the eye; and (H) bilateral developing tail tendons are seen within the posterior-most portion of the developing tail (stars). Images in F, G

24

and H are 3D reconstructions generated using Volocity, and correspond to regions indicated in the larval schematic above. Scale bars: A,B = 15 μm; C = 0.5 μm; F,G,H 1 unit = 18.51 μm; representative image of n=3 ish imaged.

(A) Schematic to illustrate the location/depth and tissues/layers involved in larval skin wounding. (B) Single and multi-channel images of wounds made to the lanks of Tg*(krt19:col1a2-GFP),* Tg*(krt19:tdTomatoCAAX)* double positive ish indicate how the epidermis (red cells) has partly healed in 20 min and completely healed over the denuded surface by 2 hours post injury (hpi), whilst collagen I (green) remains absent in this region; see also Movie 1. (C-I) Max projection confocal images of Tg*(krt19:col1a2-GFP)* transgenic ish unwounded and wounded prior to imaging at the speciied timepoints post injury (dpi); inset in C shows 3D reconstruction indicating collagen layer at 1 dpi with the collagen wound margin wrinkled where tension in this matrix meshwork has been released (arrows). E shows high magniication view of the interface between orthogonal (O) collagen wound (W) margin and newly deposited wispy collagen ibrils (arrowheads) of a 5 dpi ish. (J) Quantiication of collagen alignment index (AI) over the period of repair. For each timepoint mean of n=7-12 wounds are plotted ± SD. ns, not signiicant, **p<0.01, ***p<0.001, ****p<0.0001. (K) A 3D reconstructed, sub-epidermal view in the region of the repairing wound (red dotted line) indicates tethers extending both into muscle and between myosepta (asterisks). (L) Schematic to show tethers in addition to myosepta that remain at the healed wound site. For C-I Scale bars = 15 μm; inset in C and K, 1 unit = 24.68 μm.
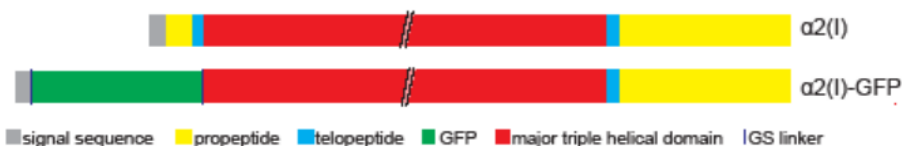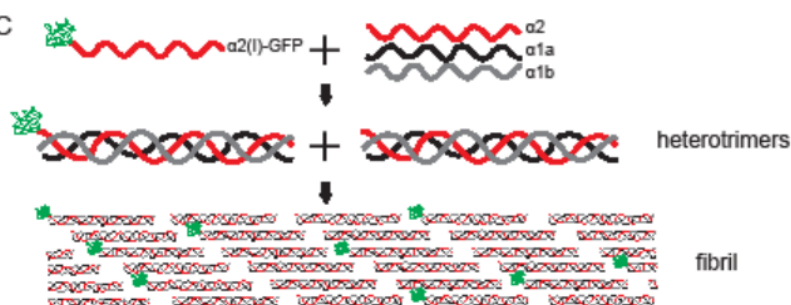
25

Figure 1

Live imaging of collagen deposition during skin development and repair in a collagen I – GFP fusion transgenic zebrafish line   19/06/2018, 11:35

26

Figure 2

27

Figure 3

28

ACCEPTED MANUSCRIPT

Highlights

29